Canadian Mineralogist
Vol. 29, pp. 461-480 (1991)

WALL-ROCK ALTERATION RELATED TO Au MINERALIZATION IN THE LOW AMPHIBOLITE FACIES: CRIXÁS GOLD MINE, GOIAS, BRAZIL

MARGARET L. THOMSON[1]
Department of Geology, The University of Western Ontario, London, Ontario N6A 5B7

ABSTRACT

The Crixás gold mine, Goias, Brazil, is an example of mesothermal deposition of gold at low-amphibolite-facies conditions. The deposit is hosted in epidote-amphibolite-facies amphibolites. Alteration assemblages in the upper ore-zone are typified by increasing abundances of ferroan dolomite, oligoclase and muscovite, and decreasing chlorite. The maximum abundance of biotite, pyrrhotite, chalcopyrite, arsenopyrite and gold occur at the reaction boundary where chlorite reacts out to ferroan dolomite and muscovite, which suggests that the processes of carbonatization and sulfidation of the host results in the reduction of gold. The presence of oligoclase in the alteration assemblage indicates low amphibolite conditions for alteration (approximately 450°C). Trapping temperatures of inclusions were found to be 440 to 480°C. Interpolated mineral equilibrium data indicate $X(CO_2)$ of the fluid of 0.31 to 0.35, and fluid-inclusion data indicate an $X(CO_2)$ of 0.15 to 0.26. Fluid salinity was relatively weak, at 7.5 to 8.1 wt.% equiv. NaCl. Alteration postdates the epidote-amphibolite-facies metamorphism and is synchronous with a S_3 fabric that truncates and overprints early nappe structures. Absolute timing of the deformation is unknown, but may be younger than Transamazonian (1000 Ma).

Keywords: Archean, greenstone belt, amphibolite, carbonitization, sulfidation, fluid inclusions, Au mineralization, Crixás gold mine, Brazil.

SOMMAIRE

Le gisement aurifère de Crixás, à Goias, au Brésil, constitue un exemple de déposition mésothermale de l'or dans le facies amphibolite inférieur. Le gisement se trouve dans un encaissant amphibolitique recristallisé dans le facies amphibolite à épidote. Les assemblages d'altération dans la partie minéralisée supérieure contiennent typiquement une quantité accrue de dolomite ferrifère, d'oligoclase et de muscovite, et montrent une diminution dans la proportion de chlorite. Les proportions maximales de biotite, pyrrhotite, chalcopyrite, arsenopyrite et or se situent à la limite de la zone à chlorite, où celle-ci est remplacée par dolomite ferrifère + muscovite, ce qui fait penser que la carbonatisation et la sulfuration des roches hôtes ont causé la réduction de l'or. La présence de l'oligoclase dans l'assemblage d'altération indique un milieu dans le facies amphibolite inférieur (environ 450°C). Les inclusions ont été piégées entre 440 et 480°C. Une interpolation des données sur les équilibres impliquant les minéraux indique une valeur $X(CO_2)$ entre 0.31 et 0.35 pour la phase fluide; les données sur les inclusions fluides indiquent une valeur $X(CO_2)$ entre 0.15 et 0.26. La salinité de ce fluide était relativement faible, entre 7.5 et 8.1. L'altération a succédé à la recristallisation métamorphique, et était synchrone au développement de la structure S_3, qui recoupe et oblitère les structures précoces en nappes. L'âge absolu de la déformation demeure méconnu, mais pourrait bien précéder l'épisode transamazonien (1000 Ma).

(Traduit par la Rédaction)

Mots-clés: archéen, ceinture de roches vertes, amphibolite, carbonatisation, sulfuration, inclusions fluides, minéralisation aurifère, gisement de Crixás, Brésil.

INTRODUCTION

Mesothermal gold deposits are commonly hosted by volcanic rocks, which vary in composition from ultramafic (*e.g.*, Kerr Addison mine, Ontario: Kishida & Kerrich 1987), to mafic (*e.g.*, Golden Mile Dolerite, Kalgoorlie, Western Australia: Phillips 1986, Clark *et al.* 1986), to andesite (*e.g.*, Sigma mine, Quebec: Robert & Brown 1986) and banded iron formation (*e.g.*, Musselwhite Prospect, Ontario: Hall & Rigg 1986). The peak regional metamorphic grade is commonly greenschist facies (Roberts 1987); however, higher-grade rocks, retrograded to the greenschist facies (*e.g.*, Calumet deposit, Quebec: Williams 1990) are not exceptional. The ore zones are characterized by an extensive, zoned alteration halo comprised dominantly of varying proportions of wall-rock minerals, and calcite, ferroan dolomite, white mica, albite and pyrite (Kerrich & Fyfe 1981, Groves & Phillips 1987, Roberts 1987). Despite the range in composition of the host rocks, the assemblages of alteration minerals are similar. This consistency in mineralogy

[1]Present address: Department of Geological Sciences, University of British Columbia, Vancouver, British Columbia V6T 2B4.

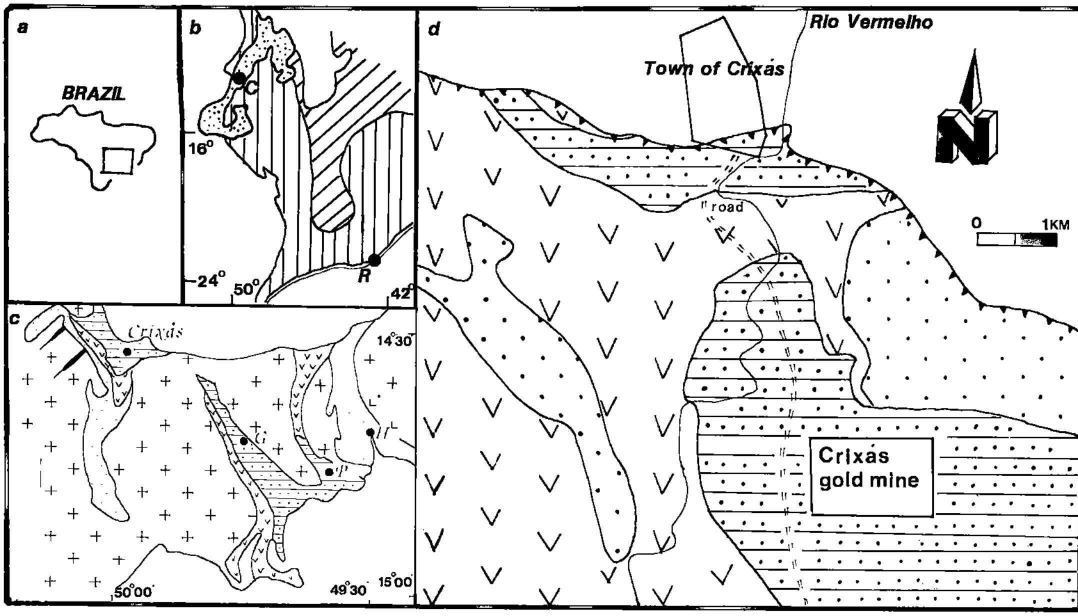

FIG. 1. a) Location of study area within Brazil. b) Location of Crixás Greenstone Belt (C) within the Goias Massif (speckled) and São Francisco Craton (diagonal stripes) and Rio de Janeiro (R). Vertical strip marks distribution of Brasiliano Cycle metamorphism (after Schobbenhaus *et al.* 1984, Fig. 1.6). c) Simplified geological map of Crixás (C), Guarinos (G) and Goias de Pilar Greenstone Belts (P) and Hidrolina (H) greenstone belts (after Saboia 1979). d) Detailed geological map of the Crixás greenstone belt within the area of the Crixás gold mine. Crosses: granite - granite gneiss terrane; stipple: meta-ultramafic rocks; "V": metamafic rocks; dashes: metasedimentary rocks; white marginal areas: Proterozoic Araxá Group (Proterozoic).

is interpreted to represent the product of interaction of a CO_2-rich fluid and the wall rocks (Fyfe & Kerrich 1984, Böhlke 1989). The volume ratio of fluid to rock is large, resulting in progressively unbuffered mineral reactions, which approach equilibrium with the CO_2-rich fluid. Studies using mineral equilibria, stable isotopes and fluid inclusions indicate that the deposition of gold occurs in P–T conditions of the middle to upper greenschist facies (350–400°C) and at mid-crustal depths (Neall & Phillips 1987, Clark *et al.* 1989, Leitch 1989, Böhlke 1989).

Rarer than the above, but nevertheless significant, is a group of mesothermal gold deposits that show that the processes of gold deposition are not solely restricted to sub-amphibolite-facies settings. Included in this group are the Eastmain River deposit, Quebec (Couture & Guha 1990), the Dahlonega Belt, southeast Georgia (Albino 1990) and Griffen's Find, Western Australia (Fare *et al.* 1990). The purpose of this study is to add to the available data on higher-temperature mesothermal gold deposits. The Crixás gold mine, Goias, Brazil (Fig. 1) provides an excellent opportunity to study alteration associated with gold deposition at conditions of the low amphibolite facies.

REGIONAL GEOLOGY AND DESCRIPTION OF THE MINE

The Crixás gold mine is located within the central portion of the Goias Massif (Fig. 1b) and is underlain by the Pilar de Goias Group of the Crixás Greenstone Belt (Figs. 1b,c, 2). The Pilar de Goias Group (Fig. 2a) is divided into the lower Corrego Alagadinho Formation, consisting dominantly of metamorphosed and deformed ultramafic lavas, locally spinifex-textured (Danni & Ribeiro 1978, Saboia 1979, Teixeira *et al.* 1981, Kuyumjian & Dardenne 1982) with subordinate mafic lavas, both intercalated with cherts and ironstones; the middle Rio Vermelho Formation, consisting of metamorphosed mafic lavas, locally pillow-lava bearing, and intercalated with cherts and ironstones, and an upper Ribeiro das Antas Formation, consisting of predominantly metamorphosed pelites, dolomites and greywackes (Saboia *et al.* 1981).

The age of the rocks of the Crixás Greenstone Belt is probably Archean. Tassinari & Montalvao (1980) dated gneiss to the immediate west of the belt at 2929 ± 105 Ma (Rb–Sr whole rock). Arndt *et al.* (1989) dated spinifex-textured metamorphosed ultramafic rocks at 2728 ± 140 Ma (Pb–Pb

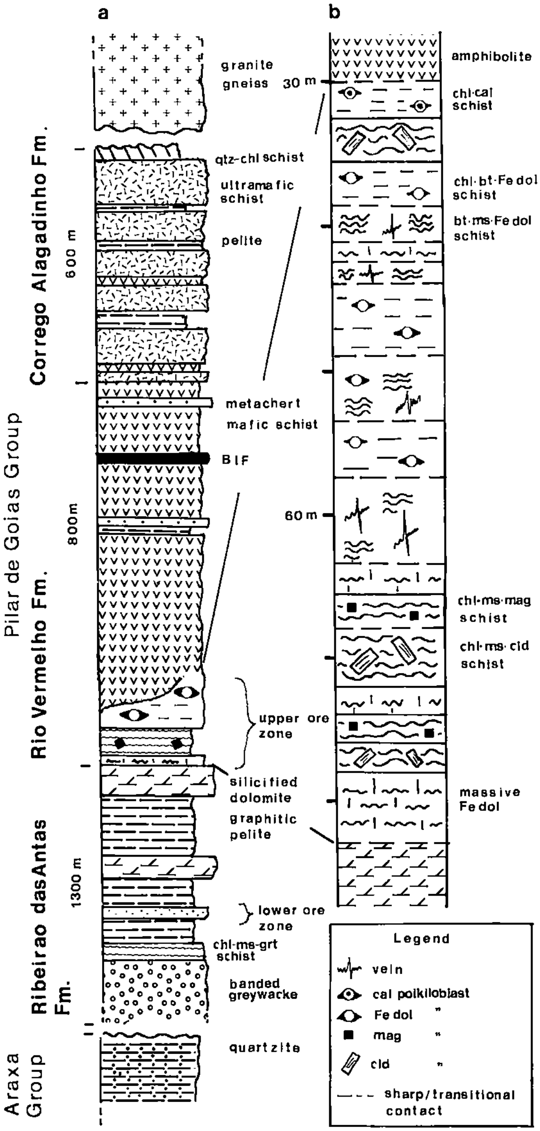

FIG. 2. a) Interpreted stratigraphic sequence of the Archean Pilar de Goias Group (modified after Kuyumjian 1981). Upper ore-zone locates the focus of this study. b) Simplified representation of sequence of lithologies through the upper ore-zone of the Crixás gold mine (depth from surface indicated to the left). Symbols: amph: amphibolite, bt: biotite, cal: calcite, chl: chlorite, cld: chloritoid, Fe dol: ferroan dolomite, grt: garnet, mag: magnetite, ms: muscovite, qtz: quartz.

whole rock), and at 2825 ± 98 Ma (Nd–Sm whole rock). The authors, however, cited evidence of unusual mobility of trace elements within the samples studied, and therefore question the age determination, cautiously concluding that an age of 2.7 Ga is reasonable.

The metamorphic and structural history of the Crixás greenstone belt is complex. Saboia (1979) and Kuyumjian (1981) described the amphibolites of the Rio Vermelho Formation as actinolite - albite - chlorite - epidote - carbonate schists; they noted the local development of the assemblage hornblende–quartz–titanite–epidote–carbonate (no feldspar mentioned). Arndt *et al.* (1989) and Thomson (1987a) described-pillow textured amphibolite as consisting of magnesio-hornblende - albite quartz - titanite - epidote with chlorite–calcite as late veins. The assemblage actinolite–albite is characteristic of greenschist-facies metamorphism of mafic rocks, whereas the assemblage hornblende–albite–epidote is characteristic of the epidote amphibolite facies (Apted & Liou 1983, Laird & Albee 1981, Moody *et al.* 1983). The distribution of rocks metamorphosed to greenschist facies and epidote amphibolite facies has not been mapped out in detail. Jost *et al.* (1991) suggested that the higher-grade rocks are restricted to zones of high strain, which is consistent with the suggestion of Thomson (1991) that assemblages formed at higher metamorphic grade represent domains of deeper-level crust thrust onto higher-level crust.

The same pod-like distribution of metamorphic isograds is reflected in the structural style of the region. Domains of undeformed spinifex-textured ultramafic rocks and pillow-lava-bearing mafic rocks are separated by domains of highly foliated and crenulated schists. Kuyumjian (1981), Thomson (1991), and Jost *et al.* (1991) agree that early folding resulted in large recumbent folds, which overturned the stratigraphy, as suggested by preserved graded bedding within conglomeratic sequences of the Ribeiro das Antas Formation (Thomson 1987a). These large-scale folds are dismembered by low-angle, high-strain zones, interpreted to represent thrusting, the timing of which is uncertain: Thomson & Fyfe (1990) and Thomson (1991) suggest that thrusting is as young as Brasiliano (450 Ma), whereas Jost *et al.* (1991) suggest that it occurred in the Archean.

The Crixás gold mine is located approximately 6 km south of the community of Crixás (Figs. 1c, d). It was discovered in 1972 by INCO Ltd., and is now owned in a joint-venture agreement between INCO Ltd. and Anglo American Ltd. The mine has recently started production, with reported reserves of 7 million tonnes at a grade of 10–12 g Au/tonne. From the structural hanging-wall to the footwall, the sequence consists of (Fig. 2b): amphibolite, dolomite, graphitic (amorphous carbon) pelite, chlorite–sericite–garnet (epidote) schist

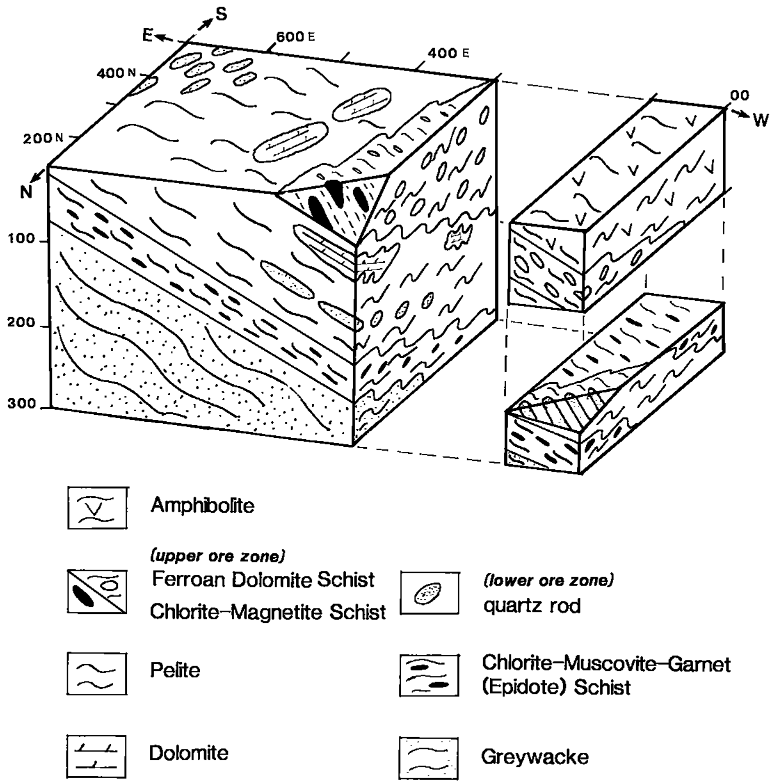

FIG. 3. Interpreted block diagram of geology of the Crixás gold mine.

and greywacke (Thomson 1986, 1987a). A block diagram of the deposit, interpreted through drill-core data, is illustrated in Figure 3. Two zones with significant Au (>2 g Au/tonne) are recognized and are termed the upper and lower ore-zones. The upper ore-zone (the focus of this study) occurs within metabasalt of the Rio Vermelho Formation at or near the contact with dolomite of the Ribeiro das Antas Formation (Figs. 2a, 3). It consists dominantly of varying assemblages of ferroan dolomite, chlorite, biotite, muscovite, oligoclase, pyrrhotite, chalcopyrite, arsenopyrite and Au (Thomson 1987b). Occurring as pods within the upper ore-zone (Fig. 2b) is a sericite–chlorite schist with porphyroblasts of chloritoid, garnet and oligoclase, which envelops a core of massive arsenopyrite, magnetite, garnet and grunerite (Thomson 1986, 1987a). The nature of this assemblage is not well understood and will not be discussed here. The lower ore zone, volumetrically more significant than the upper, occurs within graphitic (amorphous carbon) pelite at or near its lower contact and is characterized by 20–90% veins or breccia cement of quartz and minor ferroan dolomite (Thomson & Fyfe 1990, Thomson 1991).

SAMPLES STUDIED AND ANALYTICAL TECHNIQUES

All samples for this study were taken from sawn HQ (7-cm diameter) drill core, with the exception of several samples of amphibolite collected from outcrops. The latter were thin-sectioned for electron-microprobe analysis, but were not analyzed for major or trace elements, owing to the pervasive development of saprolitic weathering.

All samples chosen for geochemical analysis were carefully cut, in an attempt to remove all vein material; however, where veins are less than 1 mm wide, this was not possible. Concentrations of major and trace elements were determined by X-ray fluorescence (XRF) spectrometry with a Philips PW–1450 spectrometer. Concentrations of major elements were determined using fused rock powder of devolatilized samples (1000°C for 2 hours), following the method of Norrish & Hutton (1969). Concentrations of Na, S and the trace elements were determined using pressed powder pellets by XRF with reference to selected international standards. Concentrations of CO_2 were determined using the method of Dreimanis (1962).

Mineral compositions were determined using a

MAC 400 electron microprobe fitted with the Krisel system of automation. Routine operating conditions for silicate analysis were 15 kV accelerating current, 10-μm beam, and 20,000 counts or 30 seconds; for carbonates, 15 kV accelerating voltage, 15-μm beam and 10,000 counts or 10 seconds.

Geochemistry and Petrology of the Host Amphibolite

Documentation of the geochemistry and petrology of the host Crixás gold mine amphibolite establishes 1) an unaltered standard against which to compare the progression of alteration, and 2) the peak P–T conditions of the host rock against which to compare the P–T conditions of alteration.

Concentrations of major and trace elements for the Crixás gold mine amphibolite are summarized in Table 1. Concentrations of major and minor elements within the mine samples of amphibolite are comparable, with relatively small standard deviations for most values. Ca, Rb, and S values show the largest standard deviations, which are attributed to the presence of less than 1-mm-wide calcite veins not cut out of the sample.

Magnesio-hornblende, albite, quartz and ilmenite constitute the common assemblage of the mine amphibolite (Figs. 4b, 5, 6), with biotite and garnet (Fig. 4c) noted in a single sample. The assemblage is consistent with that described for the regionally developed amphibolite (Fig. 4a), which indicates epidote amphibolite metamorphic facies (Apted & Liou 1983, Laird & Albee 1981, Moody *et al.* 1983). The pressure conditions of metamorphism cannot be rigorously constrained. The presence of almandine garnet (Winkler 1974) and the lack of high-pressure assemblages (*i.e.*, significant crossite component in amphibole: Table 2) suggest medium-pressure metamorphic conditions.

Wallrock-Alteration Assemblages

The upper ore-zone of the Crixás gold mine is characterized by progressive alteration of the

TABLE 1. AVERAGE MAJOR OXIDE AND TRACE-ELEMENT DATA

	Crixás Au mine amphibolite (n=4)		Chl-Cal Schist (n=1)	Chl-Bt-Fe Dol Schist (n=6)		Bt-Ms-Fe Dol Schist (n=5)		Massive Fe Dol (n=5)	
	$\bar{X}$	σ	$\bar{X}$	$\bar{X}$	1σ	$\bar{X}$	1σ	$\bar{X}$	1σ
SiO_2[a]	51.21	1.3	40.95	49.09	3.3	46.27	2.9	28.79	7.0
TiO_2	1.38	0.2	0.83	1.07	0.2	1.03	0.2	0.45	0.1
Al_2O_3	11.45	1.7	9.77	12.46	2.5	12.70	2.7	6.06	2.1
FeO	14.98	1.8	8.20	12.73	2.4	11.25	1.5	11.77	5.1
MnO	0.22	0.0	0.27	0.20	0.0	0.23	0.0	0.49	0.2
MgO	6.81	1.3	3.05	8.77	1.7	9.27	0.9	19.01	2.6
CaO	9.10	3.7	34.54	11.88	3.2	15.58	3.1	31.47	4.4
Na_2O	2.08	1.2	1.39	2.16	1.4	0.89	0.6	0.31	0.4
K_2O	0.05	0.0	0.38	1.03	0.6	2.14	0.7	1.01	0.8
P_2O_5	0.13	0.0	0.14	0.10	0.0	0.12	0.0	0.43	0.6
LOI	4.99	4.8	22.29	13.81	2.5	16.85	4.3	32.51	2.5
CO_2	-	-	22.82	15.86	3.1	18.71	2.7	33.05	2.8
Nb[b]	11	8	3	25	19	15	6	19	21
Zr	87	14	40	75	17	62	13	39	18
Y	20	8	11	25	11	17	4	17	12
Sr	141	75	24	1138	39	139	21	143	71
Rb	6	11	3	39	23	48	13	31	22
As	20	7	58	310	432	450	462	104	37
Zn	103	10	37	83	14	60	18	51	11
Cu	29	9	11	22	12	35	24	11	3
Ni	30	12	18	28	12	17	7	12	5
Co	21	2	8	17	5	10	1	6	4
Cr	62	14	45	78	13	54	17	43	14
Ba	37	17	72	367	397	953	418	367	290
V	221	55	84	130	64	138	34	74	53
S	319	6	10	254	179	583	600	91	108
Ga	8	6	10	23	7	19	3	16	13

a - weight percent
Chl - chlorite
Bt - biotite
Fe Dol - ferroan dolomite
X - average
LOI - loss on ignition
b - ppm
Cal - calcite
Ms - muscovite
1σ - one standard deviation

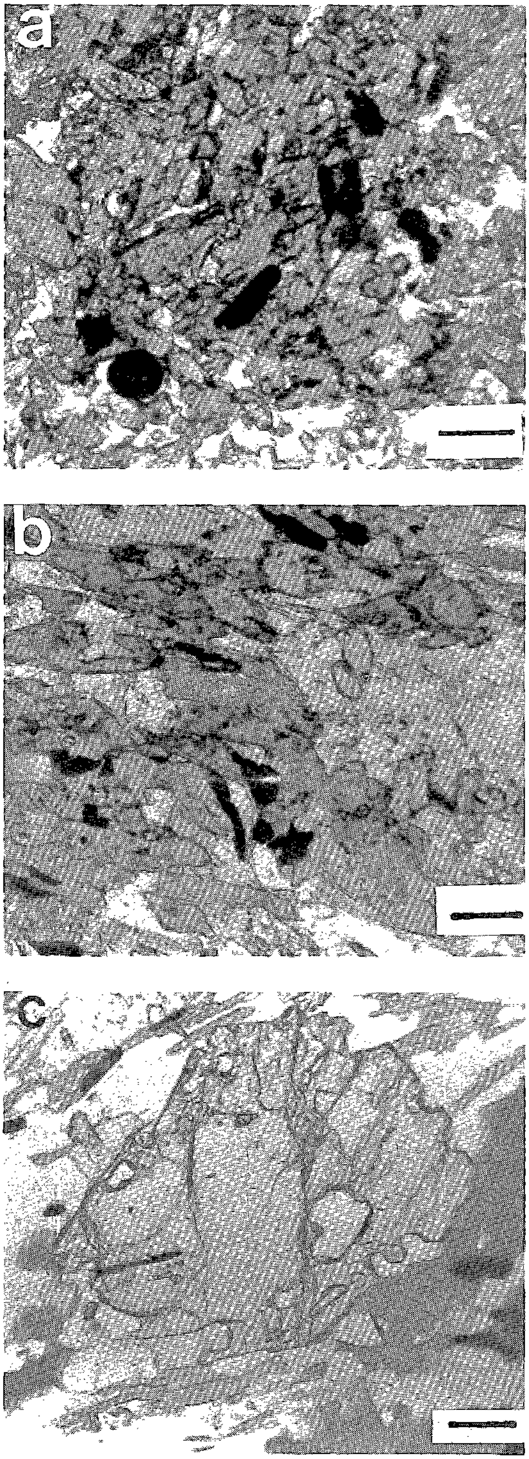

FIG. 4. Photomicrographs of: a) unaltered, equigranular regional amphibolite consisting of hornblende – albite – epidote – quartz – ilmenite (scale: 0.1 mm); b) typical incipiently altered Crixás gold mine amphibolite. Rock is moderately foliated, with chlorite overgrowing bladed hornblende and intergranular quartz, plagioclase and calcite, and stubby grains of ilmenite (scale: 500 μm); c) rare almandine garnet and biotite porphyroblast in Crixás gold mine amphibolite (scale: 500 μm).

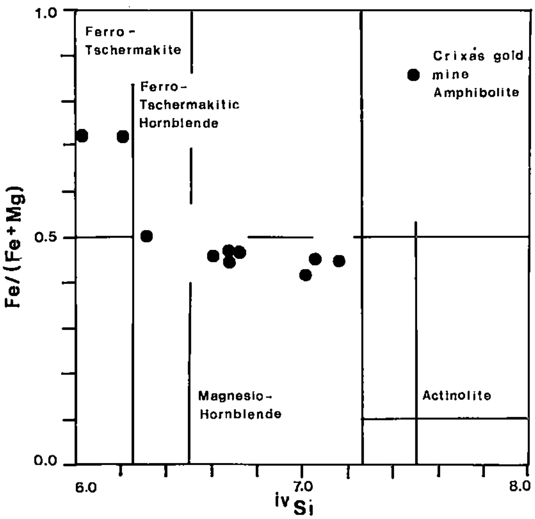

FIG. 5. Compositions of amphibole in the Crixás gold mine amphibolite.

amphibolite. Figure 7a shows a sequence of continuous core over 9.3 m that illustrates the typical appearance of progressive alteration within the upper ore-zone. Alteration zones may be symmetrically developed around veins, but are commonly dismembered by later cross-cutting veins, which makes reconstruction of the zones difficult.

Unaltered Crixás gold mine amphibolite, as described above, is rare within the study area and is generally incipiently altered. It occurs as forest green colored islands, dismembered and replaced by a grey-green chlorite–calcite schist (Figs. 7a, b). A more advanced stage of alteration (chlorite - biotite - ferroan dolomite schist) is indicated by a greenish matrix spotted by distinct black-brown porphyroblasts of biotite, blebs of pyrrhotite, 2–4 mm long diamond-shaped euhedra of arsenopyrite, and white, eye-shaped porphyroblasts of ferroan dolomite 1 to 3 mm in diameter (Figs. 7b, c). Folded grey-white ferroan dolomite - quartz veins cut and isolate patches of chlorite - biotite - ferroan dolomite schist and are lined by a grey-white biotite - muscovite - ferroan dolomite schist (Fig. 7c). The matrix along the veins commonly contains euhedra of arsenopyrite with a pressure shadow of pyr-

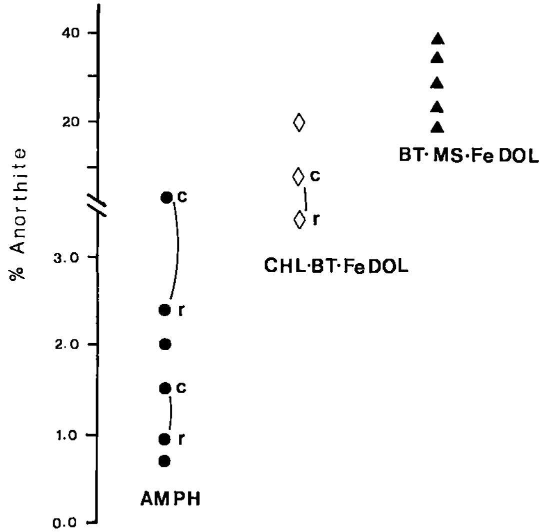

FIG. 6. Compositions of plagioclase in amphibolite and alteration assemblages.

rhotite and grains of Au (Fig. 7c). The most advanced of alteration consists of a distinct grey-buff, dominantly ferroan dolomite rock interrupted by undulose zones of white mica and chlorite, and orange-buff patches resulting from the presence of rutile (Figs. 7a, d).

MINERALOGY OF THE ALTERATION ASSEMBLAGES

The modal abundance of the dominant mineral phase is summarized in Figure 8.

Incipient alteration

Incipiently altered amphibolite in the Crixás gold mine consists of 1–2 mm wide zones of poikiloblastic magnesio-hornblende, albite, quartz and ilmenite and rare epidote, separated and replaced by anastomosing zones of chlorite, biotite, albite, calcite, quartz, ilmenite and pyrrhotite. Chlorite occurs as a rim on amphibole blades, clearly replacing the latter, and as anastomosing blades similar in size to the amphibole blades. Ilmenite occurs as blebs included in chlorite or marginal to chlorite. Calcite, quartz and untwinned albite occur as 100-μm-wide grains, matrix to the anastomosing blades of chlorite. Brown biotite occurs as porphyroblasts 1–3 mm long, commonly oblique to amphibole and chlorite blades and associated with pyrrhotite.

TABLE 2. SELECTED MICROPROBE DATA

	Amphibole	Chlorite				Biotite					Muscovite	
	Amph	Chl-Cal Schist	Chl-Bt Fe Dol Schist	Bt-Ms Fe Dol Schist	Fe Dol	Amph	Chl-Cal Schist	Chl-Bt-Fe Dol Schist	Bt-Ms-Fe Dol Schist	Fe Dol	Bt-Ms Fe Dol Schist	Fe Dol
SiO_2	26.79	24.66	24.98	24.13	23.69	32.99	35.12	35.72	36.02	37.14	48.49	45.36
TiO_2	0.08	0.14	0.06	0.13	0.10	1.66	1.59	1.69	1.96	1.59	0.38	0.32
Al_2O_3	21.06	23.23	24.17	34.31	21.07	17.17	18.20	17.86	17.33	18.53	35.31	33.38
FeO	20.63	28.02	22.98	21.97	33.06	23.09	22.32	19.17	16.79	17.77	1.81	0.13
Cr_2O_3	0.00	0.00	0.00	0.00	0.00	0.18	0.04	0.06	0.17	0.00	1.02	1.02
MnO	0.00	0.06	0.00	0.00	0.09	0.00	0.00	0.07	0.00	0.04	0.00	0.07
MgO	15.26	12.85	15.32	9.01	9.37	8.91	8.68	10.28	10.93	11.10	1.57	1.21
CaO	1.19	0.12	0.00	0.01	0.05	0.00	0.00	0.04	0.08	0.10	0.00	0.00
Na_2O	0.83	0.04	0.25	0.15	0.00	1.00	0.80	0.32	0.00	0.54	0.36	1.03
BaO	0.00	0.00	0.00	0.00	0.00	0.09	0.13	0.11	0.38	0.23	0.41	0.40
K_2O	0.08	0.00	0.12	0.01	0.00	8.50	9.22	8.80	8.96	9.08	6.57	9.30
Total	85.92	89.12	87.88	89.72	87.43	93.57	96.10	94.13	92.45	96.29	94.90	92.22
Si	5.49	5.17	5.22	5.21	5.24	5.26	5.40	5.16	5.66	5.54	6.33	6.23
^{iv}Al	2.51	2.83	2.78	2.79	2.76	2.74	2.60	2.51	2.44	2.46	1.67	1.77
^{vi}Al	2.57	2.93	2.88	2.81	2.74	0.48	0.69	0.73	0.71	0.79	3.77	3.64
Ti	0.02	0.02	0.01	0.02	0.02	0.20	0.18	0.20	0.23	0.18	0.04	0.03
Cr	0.00	0.00	0.00	0.00	0.00	0.02	0.01	0.01	0.00	0.02	0.00	0.01
Fe	3.98	4.91	4.22	6.20	6.12	3.08	2.87	2.47	2.17	2.22	0.20	0.12
Mn	0.01	0.01	0.00	0.00	0.02	0.00	0.00	0.01	0.00	0.01	0.00	0.01
Mg	5.29	4.02	4.77	2.90	3.09	2.12	1.99	2.36	2.51	2.47	0.31	0.25
Ca	0.00	0.03	0.00	0.00	0.01	0.00	0.00	0.01	0.01	0.02	0.00	0.00
Na	0.16	0.02	0.10	0.06	0.00	0.31	0.24	0.10	0.00	0.16	0.09	0.27
Ba	0.00	0.00	0.00	0.00	0.00	0.01	0.01	0.01	0.02	0.01	0.02	0.02
K	0.01	0.00	0.03	0.00	0.00	1.73	1.81	1.73	1.96	1.73	1.09	1.63

Cal - calcite
Fe Dol - ferroan dolomite
Ms - muscovite
Bt - biotite
Chl - chlorite
Amph - amphibolite

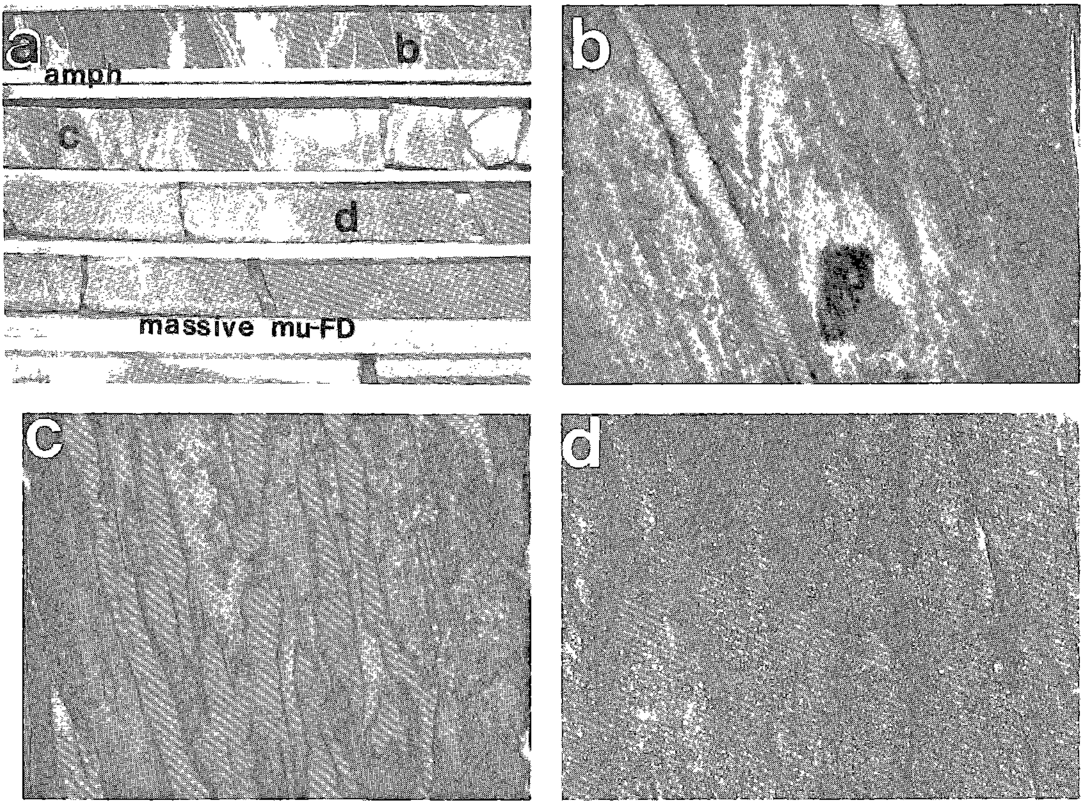

FIG. 7. Drill-core samples (7 cm in diameter). a) Complete drill-core sequence (9.3 m) through upper ore-zone; "a, b, c" refer to general location of remaining photographs. b) Chlorite–calcite schist (dark grey) with black biotite porphyroblasts, surrounded by chlorite - biotite - ferroan dolomite schist (light grey) with ferroan dolomite porphyroblasts. White quartz vein with chlorite developed at margin. c) Biotite - muscovite - ferroan dolomite schist developed at margin of ferroan dolomite - quartz veins, chlorite - biotite - ferroan dolomite schist with ferroan dolomite porphyroblasts in remainder of rock. d) Massive ferroan dolomite with typical curvilinear zones of muscovite.

Chlorite–calcite schist

In this assemblage, the anastomosing zones of chlorite, biotite, albite, calcite, quartz and pyrrhotite characteristic of incipient alteration widen to form a uniform schist (Fig. 9a). Continuous zones of anastomosing bladed chlorite (100–500 μm wide) are separated by zones of similar width of mosaic to slightly elongate grains (25–50 μm in diameter) of calcite, quartz, and untwinned albite. Blebs (5–10 μm long) of ilmenite are evenly distributed in the matrix. Calcite also occurs as composite poikiloblasts 1.5–2.5 mm wide, increasing in abundance to 25% with increasing development of the foliation (Fig. 9b). Amphibole, quartz and, rarely, plagioclase occur as inclusions in the calcite poikiloblasts. Brown biotite occurs as poikiloblasts 200–300 m long, which overgrow chlorite blades oblique to the foliation, and include quartz and albite.

Chlorite - biotite - ferroan dolomite schist

The chlorite - biotite - ferroan dolomite schist contains poikiloblasts of ferroan dolomite, biotite and oligoclase, set in a finer grained matrix of quartz, oligoclase and chlorite with minor ilmenite, pyrrhotite, chalcopyrite, arsenopyrite and tourmaline (Figs. 7b, 9c). Ferroan dolomite poikiloblasts make up composite grains up to 1.5 mm in diameter, with quartz as inclusions (Fig. 9c). Bladed biotite poikiloblasts (1–2 mm long), with inclusions of quartz and rare carbonate and chlorite, occur oblique to and seem to overgrow chlorite. Weakly color-zoned ($An_{19-3.5}$), round oligoclase porphyroblasts (500 μm in diameter) overgrow the matrix chlorite. Chlorite forms a continuous foliated mat, 50–700 μm wide (Fig. 9c). Quartz and oligoclase form equant (100 μm wide) to slightly elongate grains in a mosaic-textured matrix. Ilmenite occurs as blebs 10–20 μm long,

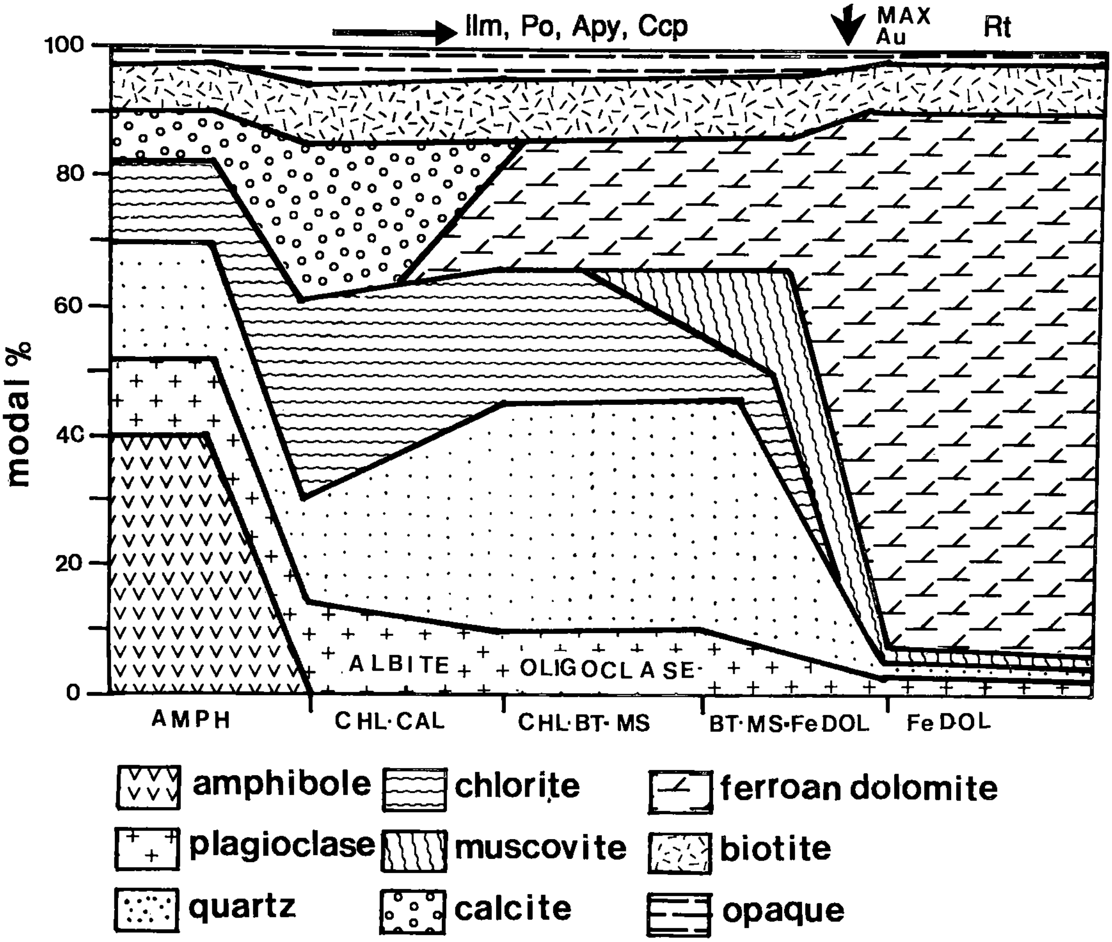

FIG. 8. Summary of modal percentage of major and minor minerals in the alteration assemblages (Ilm: ilmenite, Po: pyrrhotite, Apy: arsenopyrite, Ccp: chalcopyrite, Rt: rutile).

most commonly in the chlorite mat. Blue-green tourmaline occurs most commonly in the quartz – plagioclase – ferroan dolomite matrix and in several instances seems to replace the ferroan dolomite (Fig. 9d). Pyrrhotite and chalcopyrite occur as composite blebs, parallel to foliation and marginal to the chlorite mat. More rarely, arsenopyrite euhedra occur with pyrrhotite and chalcopyrite developed in pressure shadows. Rare flakes of gold occur at grain boundaries of quartz, with sulfides in close proximity.

Biotite – muscovite – ferroan dolomite schist

Texturally this rock unit is similar to the chlorite – biotite – ferroan dolomite schist, except that it is cut by ferroan dolomite – quartz veins and that muscovite replaces chlorite (Figs. 7c, 9e). The replacement of muscovite by chlorite is progressive, noted first at the margin of the veins. Oligoclase (An_{20-40}) occurs as porphyroblasts (Fig. 9e), up to 1 mm in diameter, that overgrow the composite muscovite – chlorite mat (Fig. 9f) and as single grains in the quartz – plagioclase – ferroan dolomite matrix. Ilmenite occurs as elongate blebs. Pyrrhotite, chalcopyrite, arsenopyrite and tourmaline are associated with trails or veinlets of biotite, quartz and ferroan dolomite 100 μm wide, which cut the matrix parallel to the foliation.

Massive ferroan dolomite

Massive ferroan dolomite consists dominantly of ferroan dolomite, muscovite and quartz (Figs. 7d, 10). Round, highly sutured (300–700 μm diameter) ferroan dolomite grains form 3–5 mm zones

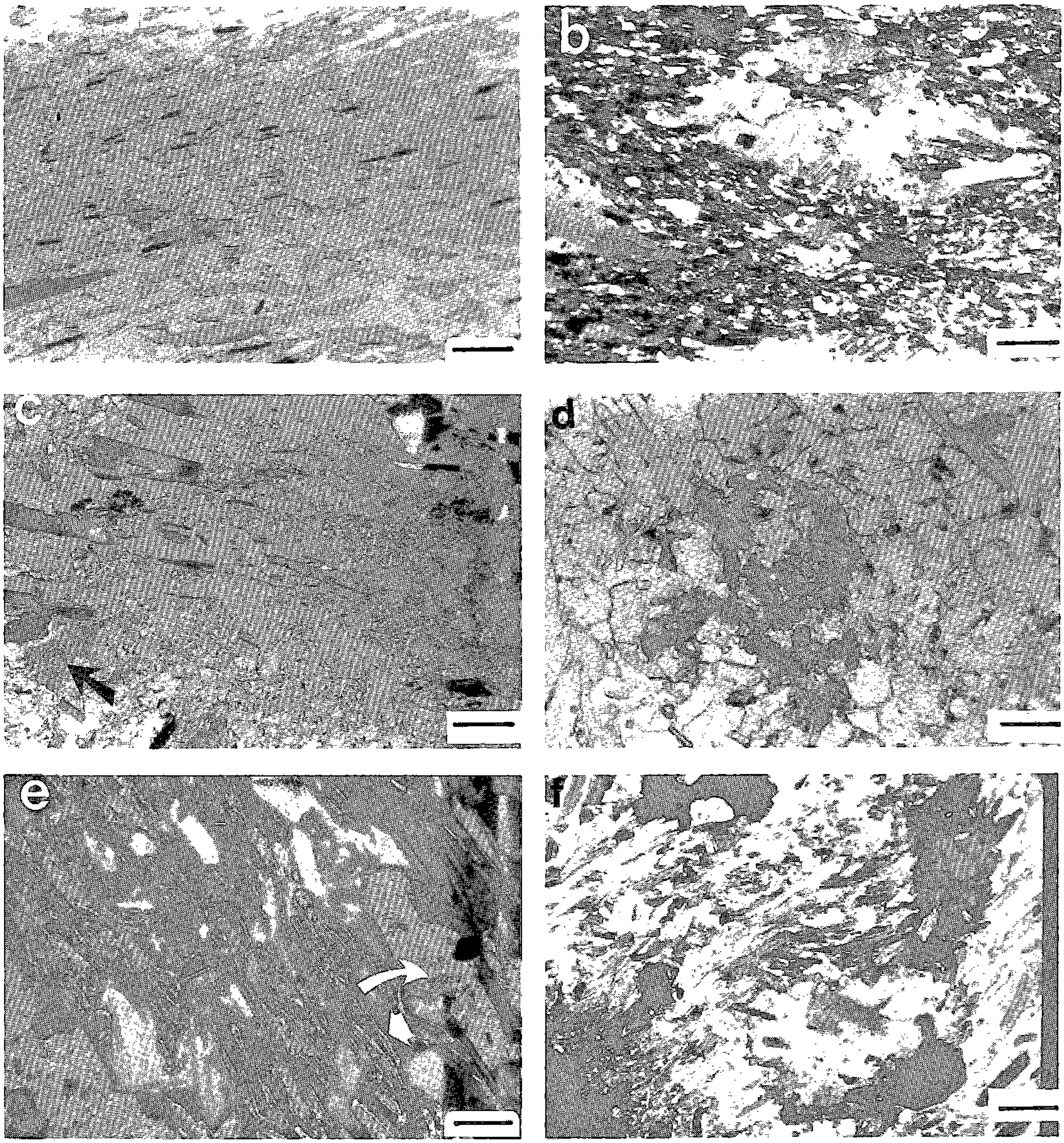

FIG. 9. Photomicrographs of alteration assemblages. a) chlorite–calcite schist: well-foliated chlorite, coarser-grained biotite in matrix of calcite–albite–quartz, stubby grains of ilmenite (scale: 500 μm, plane-polarized light). b) chlorite–calcite schist: composite calcite porphyroblast in finer-grained matrix of chlorite - calcite - albite - quartz - ilmenite (scale: 500 μm, crossed nicols). c) Chlorite - biotite - ferroan dolomite schist: chlorite forms mat interrupted by ferroan dolomite and biotite porphyroblasts, ferroan dolomite generally riddled with bubble-like quartz and ferroan dolomite inclusions (arrow) (scale: 500 μm, plane-polarized light). d) Chlorite - biotite - ferroan dolomite schist: overgrowth of tourmaline on ferroan dolomite (scale: 100 μm, plane-polarized light). e) Biotite - muscovite - ferroan dolomite schist: chlorite replaced by muscovite (thick arrow), ferroan dolomite porphyroblast riddled with inclusions (thin arrow) (scale: 100 μm, crossed nicols). f) Biotite - muscovite - ferroan dolomite schist: complete replacement of chlorite by muscovite with oligoclase porphyroblast, opaque sulfide and ilmenite (scale: 100 μm, crossed nicols).

separated by narrow (0.5 mm wide), curvilinear zones of anastomosing muscovite with minor chlorite and accessory ilmenite, rutile, oligoclase, pyrrhotite, chalcopyrite, arsenopyrite and rare gold (Fig. 10). Chlorite is replaced by muscovite, as noted, for the biotite - muscovite - ferroan

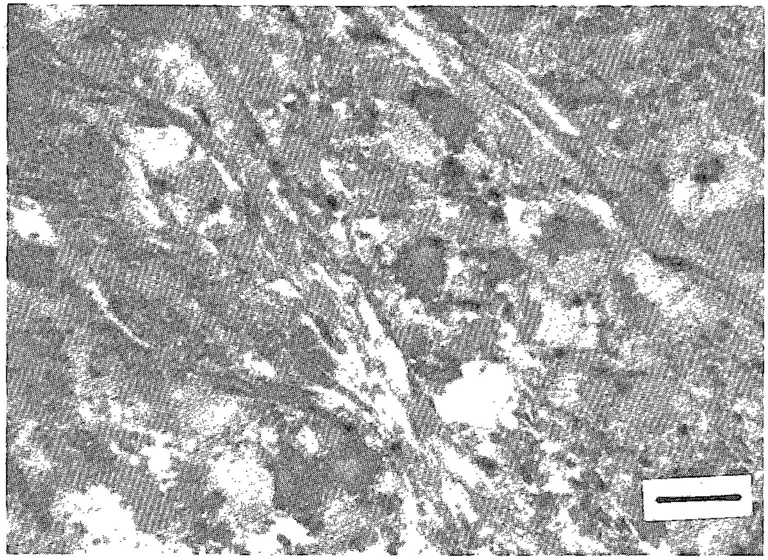

FIG. 10. Massive ferroan dolomite: muscovite forms anastomosing zones, ferroan dolomite grains are highly sutured, with development of new grains common (scale: 500 μm, crossed nicols).

dolomite schist. Oligoclase (An_{30}) porphyroblasts form within the chlorite–muscovite zones. Rutile forms needles within the muscovite-rich zones, and ilmenite occurs outside the muscovite zones, indicating a release of iron. Biotite blades, associated with arsenopyrite, pyrrhotite, and chalcopyrite, occur as trails marginal to the muscovite-rich zones.

Veins

Three types of veins have been recognized within drill core from the Crixás gold mine. Given in paragenetic order, they consist of dominantly ferroan dolomite and quartz (60 vol. %), ferroan dolomite, quartz and oligoclase (10 vol.%, Fig. 11), and quartz (30 vol. %). A significant occurrence

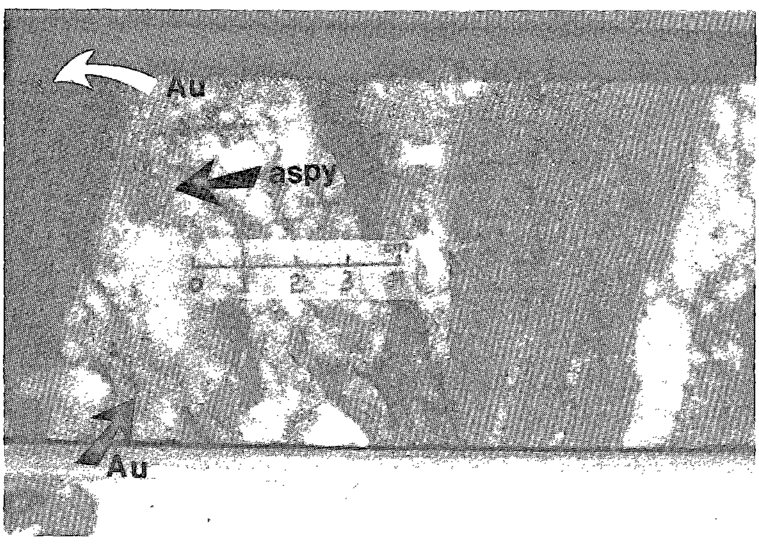

FIG. 11. Drill-core sample (7 cm diameter) of ferroan dolomite, oligoclase and quartz vein, with abundant arsenopyrite and Au. Host rock is biotite – muscovite – ferroan dolomite schist.

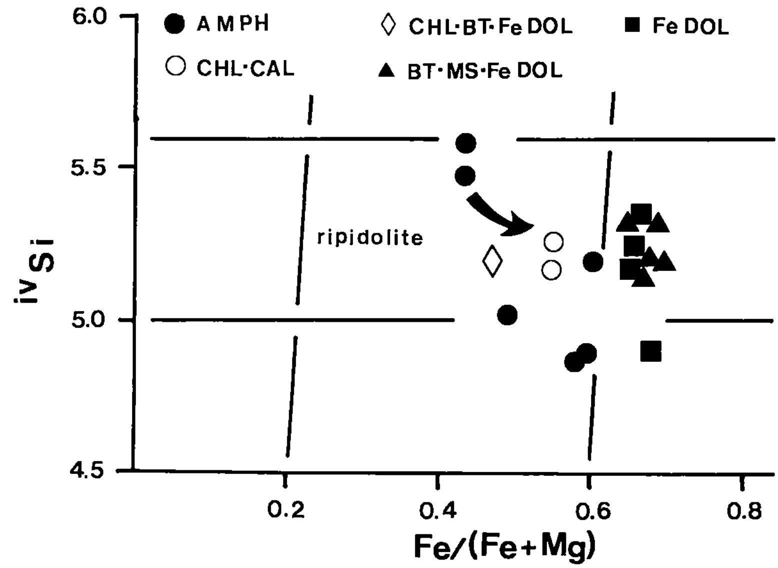

FIG. 12. Compositions of chlorite in amphibolite and alteration assemblages. Heavy arrow here and in figures to follow represents increasing degree of alteration.

of sulfides and gold occurs within and at the margin of the ferroan dolomite, quartz and oligoclase vein type. All the vein types are folded by shortening, with the axial plane parallel to the foliation direction in the matrix, and the axial hinge developed into rods parallel to the lineation direction (Fig. 7c).

Mineral Compositions

The composition of selected chlorite, carbonate, plagioclase, biotite, muscovite in the alteration assemblages is presented in Figures 6, 12, 13, 14, 15, and Table 2.

Chlorite (Fig. 12) and the carbonate minerals show an increase in Fe/(Fe+Mg) ratio with increasing alteration, with the maximum found in the biotite - muscovite - ferroan dolomite schist. The ferroan dolomite of the massive ferroan dolomite shows a wide range in Fe/(Fe+Mg) values, with the lower values associated with the presence of sulfide (Fig. 13). The Fe/(Fe+Mg) ratio of biotite (Fig. 14) and muscovite (Fig. 15) decreases with increasing degree of alteration.

Phyllosilicate minerals show a general shift toward decreasing ^{IV}Si, increasing ^{VI}Al and decrease in total Fe + Mg with increasing alteration, with the maximum found in the biotite - muscovite - ferroan dolomite schist. This is interpreted to represent a Tschermak coupled substitution, $^{IV}Si^{VI}(Fe,Mg) = {}^{IV}Al^{VI}Al$.

Barium values increase dramatically in biotite and muscovite with increase in degree of alteration (Table 2), which also results in an increase in Ca in plagioclase, from albite ($An_{0.8-2.0}$) across the miscibility gap to oligoclase–andesine (An_{15-40}).

Mass Balance

The textural and mineralogical evidence from the upper ore zone of the Crixás gold mine indicates an increase in the abundance of ferroan dolomite and sulfides at the expense of amphibole and chlorite, and to a lesser degree muscovite and biotite (Figs. 7a, 8). These changes in composition and modal abundance of minerals with alteration are accompanied by changes in the whole-rock chemistry (Table 1). In comparisons of the geochemistry of alteration, however, identical volumes of parent rock to altered product must be compared (Gresens 1967), and therefore the assumption of constant volume during alteration should be tested. Psuedomorphic replacement of original minerals commonly is used to show that no volume change has occurred during alteration (Robert & Brown 1986); however, owing to the degree of deformation associated with alteration, pseudomorphic replacement does not seem to have occurred. Ti and Zr, generally considered to be immobile during alteration, can be used to test the constancy of volume (Gresens 1967). When weight % TiO_2 is plotted against $CO_2/(CaO+MgO+FeO)$,

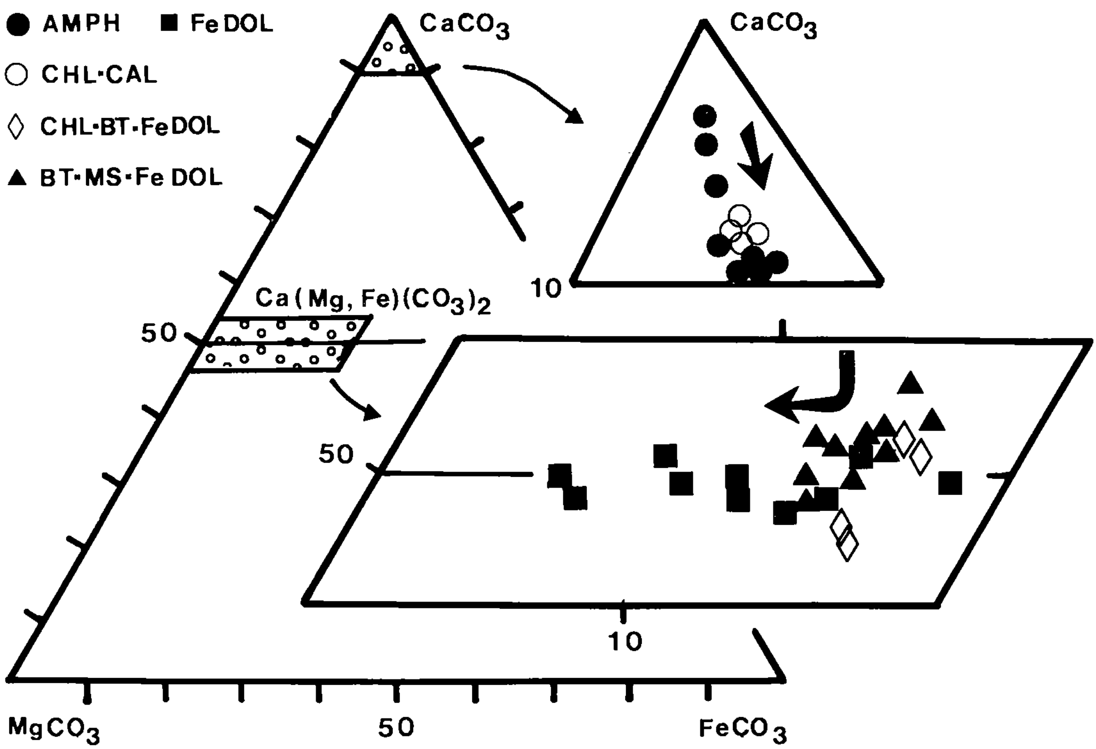

FIG. 13. Compositions of carbonate in amphibolite and alteration assemblages.

i.e., the carbonate component, there is systematic loss of TiO_2 with increase in carbonate abundance (Fig. 16). A loss in Ti is contradicted by Figure 17, where the ratio of weight % TiO_2 to Zr is relatively constant for the various assemblages. The apparent

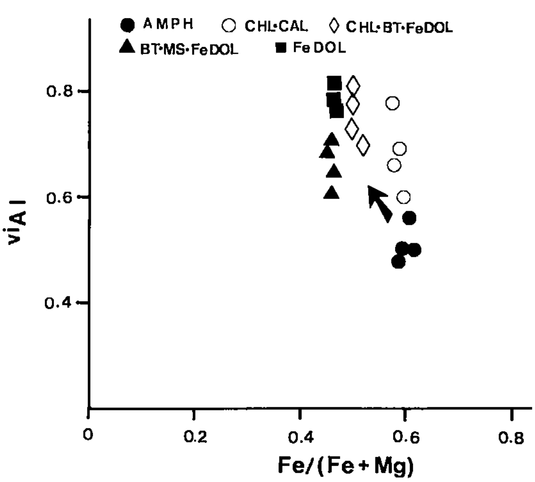

FIG. 14. Compositions of biotite in alteration assemblages.

loss in Ti with alteration would therefore suggest a relative gain in volume to, in effect, dilute the concentration of Ti. Kerrich & Fyfe (1981) pointed out that volume increases are required for the reactions related to carbonatization. The calculated volume-factors of the elements Ti, Al and Zr commonly cluster, and the average values are used to calculate the volume factors. The volume factors all show an increase in volume relative to the amphibolite. The volume factors used were 1.58 for chlorite–calcite schist, 1.25 for chlorite - biotite - ferroan dolomite schist, 1.16 for biotite - muscovite - ferroan dolomite schist, and 2.82 for massive ferroan dolomite.

Table 3 summarizes the gains and losses (in %) of various elements for the alteration assemblages, as compared against the Crixás gold mine amphibolite sample 159–1. Each alteration assemblage shows consistent gains in Ca, Sr, and Ba, reflecting the increase in carbonate and phyllosilicates. Mg, As, and S increase with the degree of alteration, and Fe gains are most significant in the massive ferroan dolomite. Si shows variable gains and losses, perhaps reflecting the presence or absence of quartz-bearing veins less than 1 mm wide, which were not removed from the samples. V and Cu are

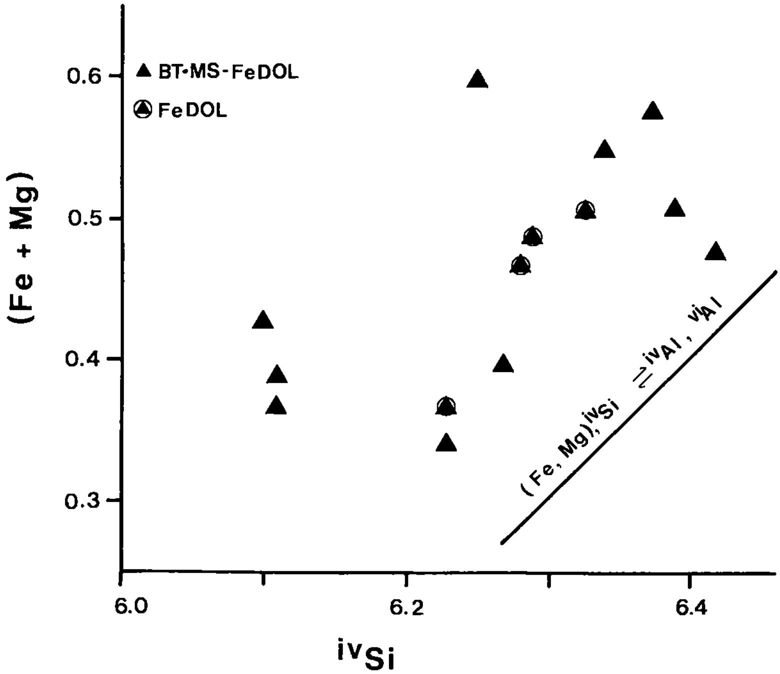

FIG. 15. Compositions of muscovite in alteration assemblages.

lost in chlotite–calcite schist and chlorite – biotite ferroan dolomite schist, but gained in biotite –

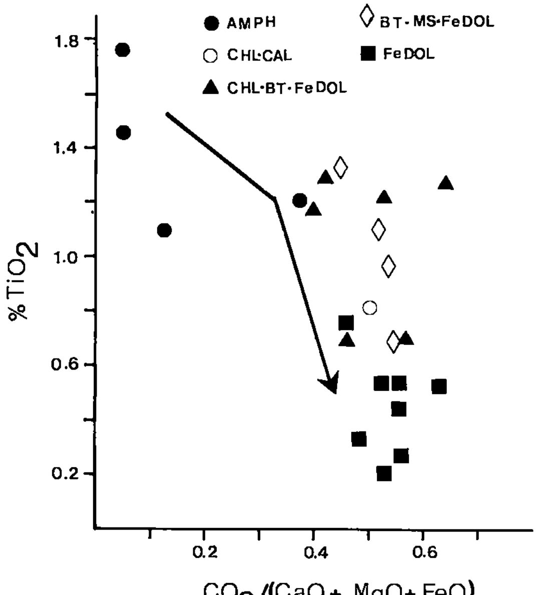

FIG. 16. TiO_2 – CO_2/(CaO + MgO + FeO) plot illustrating reverse relationship within Crixás gold mine amphibolite and alteration assemblages.

muscovite – ferroan dolomite schist. Losses in Na, Ni, Co and Zn are consistent in all the alteration assemblages.

FLUID INCLUSIONS IN VEIN QUARTZ

A preliminary study was carried out of fluid inclusions found in three doubly polished samples of ferroan dolomite and quartz veins that cross-cut biotite – muscovite – ferroan dolomite schist. Thermometric data were obtained on fluid inclusions in quartz using an adapted Chaixmecha heating and freezing stage (Poty *et al.* 1976). Although not comprehensive, these data provide independent information on the temperature and composition of the fluid. The largest population of fluid inclusions are secondary, as trails clearly cross-cut grain boundaries (70%). Pseudoprimary inclusions form distinct trails or clusters limited to a single grain (30%). Primary inclusions were not confidently identified. The pseudoprimary inclusions are small, ranging from <1 to 5 μm, and contain three phases, H_2O-rich liquid, CO_2-rich liquid and H_2O-CO_2-rich vapor. The volumetric proportions of the CO_2-rich liquid range from 40 to 60%. The homogenization of CO_2 to the liquid phase was found to range from 28.3° to 30.3°C, consistent with a CO_2-rich vapor. Clathrates formed in all inclusions upon heating of frozen

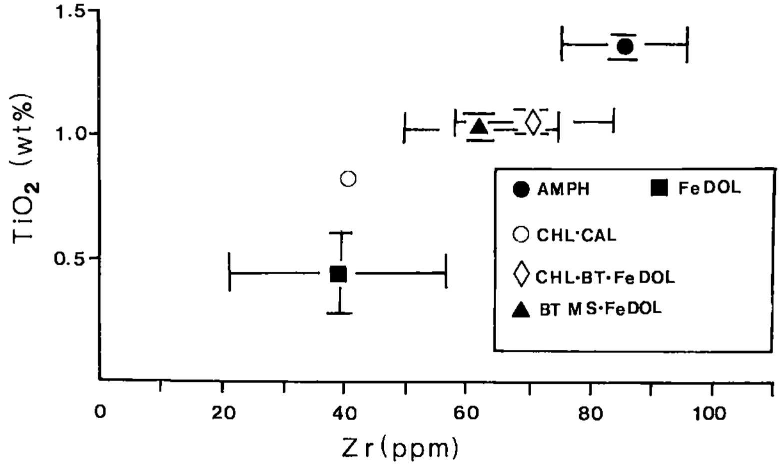

FIG. 17. TiO_2-Zr diagram (Floyd & Winchester 1975) illustrating consistent ratios between Crixás gold mine amphibolite and alteration assemblages.

CO_2-bearing inclusions, and melt at 5.6° to 6.0°C. Homogenization temperatures were difficult to determine as decrepitation commonly occurred prior to homogenization. In those few inclusions (n = 7) where homogenization temperatures were determined, the values ranged from 442° to 488°C.

Limited interpretation of the trapping temperature and composition of the fluid can be made from these data. The trapping temperatures are above 440° and probably below 500°C. The composition of the fluid is weakly to moderately saline (7.5 to 8.1 equivalent wt.% NaCl). The $X(CO_2)$ ranges between 0.15 and 0.26, based on a range of volume of 40 to 60% (Roedder 1984, Parry 1986).

DISCUSSION OF ALTERATION

Alteration assemblages and the boundaries between alteration zones have been described as isograds, and general reactions have been proposed to describe these boundaries within greenschist facies mesothermal gold deposits (Clark *et al.* 1986, Neall & Phillips 1987). Two summary reactions are:

1) 3 actinolite + 2 zoisite + 8 H_2O + 10 CO_2 → 3 chlorite + 10 calcite + 21 quartz,

which defines the boundary between the unaltered Crixás gold mine amphibolite and incipiently altered and chlorite–calcite schist, and,

2) biotite + chlorite + 8 calcite + 8 CO_2 → muscovite + 8 dolomite + 3 quartz + 4 H_2O,

which defines the boundary between chlorite–calcite schist and massive ferroan dolomite. The extent to which the reaction goes to completion depends on the availability of the reacting fluid. The occurrence of massive ferroan dolomite strongly suggests that 1) the fluid-to-rock ratio was very high, and 2) the reaction went to completion, consuming all the reactants.

The changes in the mineral chemistry and whole-rock compositions are a consequence of these reactions. Mass-balance calculations indicate relatively small gains in iron to account for the increase in Fe/(Fe + Mg) ratio of chlorite, calcite and ferroan dolomite with progressive alteration (Figs. 12, 13). Increases in Fe, therefore, must be the result of a relative decrease in Mg values, due to the formation of ferroan dolomite. As well, the decrease in the modal abundance of chlorite (Fig. 8) reduces the amount of Fe required to increase the Fe/(Fe + Mg) ratio. The total Fe + Mg of the phyllosilicates decreases with progressive alteration, yet the mass-balance calculations suggest increases in Mg and, to a lesser extent, Fe. This can be explained, in part, by an increased abundance of ferroan dolomite, which accommodates Mg and Fe. The maximum modal abundance of sulfides (arsenopyrite, pyrrhotite and chalcopyrite) and Au occurs within the biotite – muscovite – ferroan dolomite schist near the boundary with massive ferroan dolomite, which suggests that Fe is progressively partitioned into the sulfides. This reaction boundary also marks a dramatic decrease in Fe within muscovite and ferroan dolomite, thereby liberating Fe for the formation of sulfides.

The process of carbonatization and related sulfidation is one that has been documented in many mesothermal gold deposits, and Crixás is not

TABLE 3. MASS BALANCE: PERCENT GAINS AND LOSSES RELATIVE TO PARENT AMPHIBOLITE

	159-1 Amph	Chl-Cal Schist	Chl-Bt-Fe Dol Schist		Bt-Ms-Fe Dol Schist		Massive Fe Dol	
		n=1	n=6		n=5		n=5	
ρ	2.98	2.83	2.83		2.83		3.07	
V_f		1.58	1.25		1.16		2.82	
		X_i	$\bar{X}_i$	1σ	$\bar{X}_i$	1σ	$\bar{X}_i$	1σ
SiO_2[a]	51.55	9.9	-6.4	19.3	3.5	12.8	19.3	30.0
TiO_2	1.10	0.1	0.0	0.0	0.0	0.1	0.0	0.4
Al_2O_3	14.07	0.5	-0.3	0.6	1.5	3.0	-0.7	1.9
FeO	14.28	-1.9	0.2	4.3	0.6	4.4	19.6	20.7
MnO	0.18	0.2	0.0	0.0	0.2	0.2	0.9	0.6
MgO	8.78	-4.2	1.9	5.2	9.2	14.2	35.1	12.3
CaO	7.63	44.2	6.9	7.2	23.5	23.3	63.3	17.2
Na_2O	3.15	-1.0	-0.9	1.3	-2.2	0.5	-2.8	0.2
K_2O	0.01	0.5	1.1	0.6	2.8	1.2	1.8	0.1
P_2O_5	0.09	0.1	0.0	0.0	0.2	0.3	0.3	0.1
Nb[b]	12	-8	20	37	1	9	15	15
Zr	72	-11	16	39	-6	9	5	13
Y	16	0	13	19	3	4	15	12
Sr	106	230	51	59	118	133	128	84
Rb	<2	3	50	44	50	62	55	30
As	18	68	312	403	366	370	128	30
Zn	98	-43	-0	34	-25	16	26	59
Cu	35	-18	-11	10	1	27	-9	6
Ni	48	-20	-14	20	-29	5	-21	10
Co	23	-12	-4	4	-12	1	-4	17
Cr	78	-10	16	39	16	10	26	40
Ba	17	540	461	593	1155	450	712	494
V	182	-57	-49	54	25	22	29	183
S	177	47	149	162	354	501	241	473
Ga	11	4	16	16	11	4	13	7

a - weight percent; b - ppm
Amph - amphibolite; Fe Dol - Ferroan Dolomite
Chl - chlorite; ρ - density (g/cm^3)
Cal - calcite; V_f - volume factor
Bt - biotite; X_i - average
Ms - muscovite; 1σ - one standard deviation

an exception. Studies such as those by Neall & Phillips (1987), Leitch (1989) and Böhlke (1989) show that this process has a direct consequence on the deposition of gold. The reduction of gold is interpreted to result from oxidation of Fe^{2+} to form pyrite:

$$Au^{2+} + Fe^{2+} S^0_g \rightleftharpoons Au^0 + 2e^- + FeS_2^{2-},$$

where Fe^{2+} is decoupled from silicate minerals through the formation of ferroan dolomite and sulfides. Pyrite, however, is not associated with gold in the alteration assemblages of the Crixás gold deposit, and therefore, the gold–pyrite redox couple cannot be suggested here. At higher temperatures and pressures, another redox reaction couple may be important. Romberger (1986) suggested the redox couple:

$$2\,AuAsS_2^0 + 2\,Fe^{2+}\,2\,H_2O \rightleftharpoons 2\,Au + 2\,FeAsS + 4\,H^+ + O_2 + S_2,$$

where arsenopyrite is common in the ore assemblage. No data are available on the stability of the thioarsenide complex; however, deposits such as Crixás indicate that future work should look at this problem.

P–T–X

The appearance of oligoclase in a mafic assemblage is a function of temperature and not of increasing $X(CO_2)$ (Carmichael 1984). It is sensitive to pressure and is displaced to higher temperatures with increasing pressure. Under conditions of 3 kbar, the isograd for the first appearance of oligoclase is approximately 450°C. This temperature is corroborated by the few determinations of fluid inclusion homogenization, between 440° and 500°C. No attempt has been made to calculate the $X(CO_2)$ using thermodynamics; however, interpolation of the T–$X(CO_2)$ diagram presented by Clark *et al.* (1986) for reaction (2) at 3 kbar and 450°C gives a $X(CO_2)$ range of 0.31 to 0.35. The fluid inclusions suggest a relatively low-salinity fluid with a $X(CO_2)$ value of 0.15 to 0.26. The pressure is not constrained, but given the temperatures and assuming a normal geothermal gradient, a pressure of 3 kbar is not unreasonable.

Table 4 summarizes the available data on P–T–*X* conditions in several gold deposits and those interpreted for the Crixás gold mine. The Victory mine, Hunt mine, Bralorne and Alleghany deposits represent deposition of gold under greenschist-facies conditions. There, the pressure was 1 to 2

TABLE 4. SUMMARY OF P-T-X CONDITIONS

	Crixás	Dahlonega[1]	Alleghany[2]	Bralorne[3]	Hunt[4]	Victory[5]
P (kbar)		3 (?)	>4.5-6	2.1	1.0-1.75	0.8-1.8,1.7-2.0
T (°C)(FI)	440-480	n/a	325±50	350	280-350	370±30
(cal.)	450-500	450-500	n/a	n/a	350-400	390±40
X(CO2)(FI)	0.15-0.26	0.25-0.30	n/a	0.05-0.15	0.25	0.1-0.2
(cal.)	0.31-0.36	n/a	0.1	1	0.18-0.24	0.12-0.26
sal. (FI)	7.5-8.1	n/a	2	1-3	2	8.0-9.0

1 Albino (1990)
2 Böhlke (1989)
3 Leitch (1989)
4 Neall & Phillips (1987)
5 Clark *et al.* (1989)

n/a - not available
sal. - salinity: equivalent weight percent NaCl
FI - fluid inclusion data
cal. - calculated from mineral equilibria

kbar, and the temperature averaged about 350°C. The fluid was weakly saline, 2–8 equivalent wt.% NaCl. The $X(CO_2)$ is constrained by mineral equilibria and fluid inclusion studies and ranged from 0.12 to 0.26. Data on deposits from the Dahlonega Belt indicate that these deposits formed under amphibolite-facies conditions. The pressure, temperature and $X(CO_2)$ are elevated compared to those of the greenschist-facies group, but compares well to the Crixás gold mine, with perhaps the exception of the $X(CO_2)$. The interpolated $X(CO_2)$ based on reaction (2) indicates a range of 0.31 to 0.35, a similar range to that indicated by the Dahlonega Belt data, but the fluid inclusion values are more comparable to the Victory mine data. A more thorough study of the fluid inclusions and treatment of the mineral equilibria would provide more reliable information.

Timing of Alteration

The petrographic and mineral chemistry evidence indicates that alteration postdated epidote amphibolite metamorphism. Evidence from the structurally lower unit, the Graphitic Pelite, in the form of S_3, a strong planar fabric, that weakly wraps around peak-metamorphic garnet porphyroblasts, indicates that deformation continued after the nucleation of the peak mineral assemblage (Thomson & Fyfe 1990, Thomson 1991). Incipient alteration, consisting of zones of chlorite–calcite schist, are parallel to S_3, suggesting a structural control of the early stages of alteration. Chlorite, biotite and muscovite within the more advanced alteration assemblages are oriented subparallel or parallel to S_3. The three vein types are all folded, with their axial plane parallel to S_3. These data provide strong evidence that deformation and alteration are synchronous with the development of the strong S_3 fabric.

The association of veining, alteration and deformation must be included in any model of genesis of the upper ore-zone of the Crixás gold mine. Interpretations of mesothermal gold deposits suggest that veining, alteration and deformation are related to progressive deformation and fluid ingress along regionally significant zones of ductile shear. A similar interpretation is suggested for the upper ore-zone of the Crixás gold mine, where the pronounced planar fabric of S_3 is an L–S fabric related to low-angle thrusting.

The absolute timing of alteration and deformation is not known. Jost *et al.* (1991) suggested that alteration and deformation are limited to the Archean. M. Harrison obtained a plateau age of about Transamazonian Cycle age, 1000 Ma (no precision indicated) on an amphibole from the Rio Vermelho Formation metabasalt, using the $^{40}Ar/^{39}Ar$ method (N. Arndt, written comm., June 1989). Thomson & Fyfe (1990) and Thomson (1991) suggest that thrusting may be as young as 450–700 Ma (Brasiliano Cycle). Clearly this issue cannot be resolved without detailed age dating of metamorphic and metasomatic minerals.

Conclusions

The host Crixás gold mine amphibolite is metamorphosed to conditions of the epidote amphibolite facies. Alteration related to Au-mineralization postdates the epidote amphibolite facies metamorphism.

The assemblage of alteration minerals shows an increase in ferroan dolomite and muscovite, and decrease in chlorite and biotite. The Fe/(Fe+Mg) ratio generally decreases with progressive alteration. This assemblage is not unlike that seen in many greenschist-facies mesothermal gold deposits, with the exception of the presence of oligoclase rather than albite and pyrrhotite rather than pyrite.

The mass-balance calculations suggest that the process of alteration does not represent large gains in Fe or Mg, and is dominated by the redistribution Fe and Mg from the phyllosilicate phases to ferroan dolomite and sulfides. Gold precipitation is a direct consequence of the alteration process, possibly resulting from a coupled redox reaction involving Fe^{2+}.

The conditions of alteration correspond to the low amphibolite facies, as determined by the mineral assemblage and fluid inclusions. Oligoclase is sensitive to temperature and insensitive to pressure; it forms at the greenschist–amphibolite facies transition, interpreted to be approximately 450°C. Trapping temperatures, although few, suggest that the temperature of veining was approximately 450°C. The pressure cannot be rigorously constrained, but is considered to be 3 kbar, assuming a normal geothermal gradient. Salinity of the fluid is 7.5–8.1 equivalent wt.% NaCl. $X(CO_2)$ based on interpolated mineral equilibria ranged from 0.31 to 0.35, whereas fluid inclusion data suggest lower values, 0.15–0.26. The former is favored.

Alteration is synchronous with deformation. The deformation is related to low-angle thrusting that truncates early nappe structures. The absolute timing of alteration is unknown, but may be as young as Brasiliano age (450–750 Ma).

Acknowledgements

INCO Ltd., in particular Mr. T. Podolsky and Dr. J.P. Golightly, provided the opportunity and encouragement to work on the Crixás gold mine. At the University of Western Ontario, Professor W.S. Fyfe and Dr. G.V. Albino influenced many of the ideas presented here. Analytical assistance was provided by R. L. Barnett, C. Wu and J. Forth. Drafts of this paper were greatly improved through the criticisms of Drs. E.C. Prosh, F. Robert, G.N. Phillips, T.H. Brown and R.F. Martin.

References

ALBINO, G.V. (1990): Fluid sources for "break"-type gold deposits - What do we really know? *In* NUNA Research Conference on Greenstone Gold and Crustal Evolution (F. Robert & S.B. Green, eds.). *Geol. Assoc. Can. - Soc. Econ. Geol.*, 11-12 (abstr.).

APTED, M.J. & LIOU, J.G. (1983): Phase relations among greenschist, epidote-amphibolite and amphibolite in a basaltic system. *Am. J. Sci.* **283-A**, 328-354.

ARNDT, N.T., TEIXEIRA, N.A. & WHITE, W.M. (1989): Bizarre geochemistry of komatiites from the Crixás greenstone belt, Brazil. *Contrib. Mineral. Petrol.* **101**, 187-197.

BÖHLKE, J.K. (1989): Comparison of metasomatic reactions between a common CO_2-rich vein fluid and diverse wall rocks: intensive variables, mass transfers, and Au mineralization at Alleghany, California. *Econ. Geol.* **84**, 291-327.

CARMICHAEL, D.M. (1984): Mineral equilibria in metabasites and metagreywackes in the transition from greenschist to amphibolite facies. *Geol. Soc. Am., Abstr. Programs* **16**, 464.

CLARK, M.E., ARCHIBALD, N.J. & HODGSON, C.J. (1986): The structural and metamorphic setting of the Victory gold mine, Kambalda, Western Australia. *In* Proc. Gold '86, an International Symp. on the Geology of Gold (A.J. Macdonald, ed.). Konsult Intern. Inc., Toronto, Ontario (243-254).

______, CARMICHAEL, D.M., HODGSON, C.J. & FU, F. (1989): Wall-rock alteration, Victory gold mine, Kambalda, Western Australia: processes and P-T-X_{CO2} conditions of metasomatism. *In* The Geology of Gold Deposits: the Perspective in 1988 (R.R. Keays, W.R.H. Ramsay & D.I. Groves, eds.). *Econ. Geol., Monograph* 6, 445-459.

COUTURE, J.-F. & GUHA, J. (1990): The Eastmain River deposit: a syntectonic shear zone hosted vein-type gold deposit in an amphibolite grade setting. *In* NUNA Research Conference on Greenstone Gold and Crustal Evolution (F. Robert & S.B. Green, eds.). *Geol. Assoc. Can. - Soc. Econ. Geol.*, 26 (abstr.).

DANNI, J.C.M. & RIBEIRO, C.C. (1978): Caracterizacao estratigrafica da sequencia vulcano-sedimentar de Pilar de Goias e de Gurarinos, Goias. *Anais XXX Congresso Brasileiro Geologia, Recife* **2**, 582-596.

DREIMANIS, A. (1962): Quantitative gasometric determinations of calcite and dolomite using Chittick apparatus. *J. Sed. Petrol.* **29**, 520-529.

FARE, R.J., GROVES, D.I. & MCNAUGHTON, J.J. (1990): A syn-metamorphic, lower-granulite facies, lode-gold deposit at Griffin's Find, Western Australia: implications for sources of Archaean auriferous fluids. *In* NUNA Research Conference on Greenstone Gold and Crustal Evolution (F. Robert & S.B. Green, eds.). *Geol. Assoc. Can. - Soc. Econ. Geol.*, **37** (abstr.).

FLOYD, P.A. & WINCHESTER, J.A. (1975): Magma type and tectonic setting discrimination using immobile elements. *Earth Planet. Sci. Lett.* **27**, 211-218.

FYFE, W.S. & KERRICH, R. (1984): Gold: natural concentration processes. *In* Gold '82: the Geology, Geochemistry and Genesis of Gold Deposits (R.P. Foster, ed.). *Geol. Soc. Zimbabwe, Spec. Publ.* **1**, 99-127.

GRESENS, R.L. (1967): Composition-volume relationships of metasomatism. *Chem. Geol.* **2**, 47-65.

GROVES, D.I. & PHILLIPS, G.N. (1987): The genesis and tectonic control on Archaean gold deposits of the Western Australian Shield - a metamorphic replacement model. *Ore Geol. Rev.* **2**, 287-322.

HALL, R.S. & RIGG, D.M. (1986): Geology of the West Anticline Zone, Musselwhite prospect, Opapimiskan Lake, Ontario, Canada. *In* Proc. Gold '86, an International Symp. on the Geology of Gold (A.J. Macdonald, ed.). Konsult Intern. Inc., Toronto, Ontario (124-136).

JOST, H., DANNI, J.C.M., DE OLIVEIRA, A.M., DO CRAVO BARROS, J.G. & YAKOKA, W. (1991): Geological outline and mineral deposits of the Archean Crixás region, central Brazil. *Brazil '91 Field Excursion Guide.*

KERRICH, R. & FYFE, W.S. (1981): The gold-carbonate association: source of CO_2, and CO_2 fixation reactions in Archaean lode deposits. *Chem. Geol.* **33**, 265-294.

KISHIDA, A. & KERRICH, R. (1987): Hydrothermal alteration zoning and gold concentration at the Kerr-Addison Archean lode gold deposit, Kirkland Lake, Ontario, Canada. *Econ. Geol.* **82**, 649-690.

KUYUMJIAN, R.M. (1981): *Geologia e Mineralizacoes*

Aurifers do "Greenstone belt" da Faixa Crixás - Go. M.Sc. thesis, Univ. Brasilia, Brasilia, Brasil.

______ & DARDENNE, M.A. (1982): Geochemical characteristics of the Crixás Greenstone Belt, Goias, Brazil. *Revista Brasileira de Geociencias* **12**, 324-330.

LAIRD, J. & ALBEE, A.L. (1981): Pressure, temperature, and time indicators in mafic schists: their application to reconstructing the polymetamorphic history of Vermont. *Am. J. Sci.* **281**, 127-175.

LEITCH, C.H.B. (1989): *Geology, Wallrock Alteration, and Characteristics of the Ore Fluid at the Bralorne Mesothermal Gold Vein Deposit, Southwestern British Columbia.* Ph.D. thesis, Univ. British Columbia, Vancouver, British Columbia.

MOODY, J.B., MEYER, D. & JENKINS, J.E. (1983): Experimental characterization of the greenschist/amphibolite boundary in mafic systems. *Am. J. Sci.* **283**, 48-92.

NEALL, F.B. & PHILLIPS, G.N. (1987): Fluid - wall rock interaction in an Archean hydrothermal gold deposit: a thermodynamic model for the Hunt mine, Kambalda. *Econ. Geol.* **82**, 1679-1694.

NORRISH, K. & HUTTON, J.T. (1969): An accurate X-ray spectrographic method for the analysis of a wide range of geological samples. *Geochim. Cosmochim. Acta* **33**, 431-453.

PARRY, W.T. (1986): Estimation of X_{CO2}, P, and fluid inclusion volume from fluid inclusion temperature measurements in the system $NaCl-CO_2-H_2O$. *Econ. Geol.* **81**, 1009-1013.

PHILLIPS, G.N. (1986): Geology and alteration in the Golden Mile, Kalgoorlie. *Econ. Geol.* **81** 779-808.

POTY, B., LEROY, J. & JACHIMOWICZ, L. (1976): Un nouvel appareil pour la mesure des températures sous le microscope: l'installation de microthermométrie Chaixmeca. *Bull. Soc. Fr. Minéral. Cristallogr.* **99**, 182-186.

ROBERT, F. & BROWN, A.C. (1986): Archean gold-bearing quartz veins at the Sigma mine, Abitibi greenstone belt, Quebec. II. Vein paragenesis and hydrothermal alteration. *Econ. Geol.* **81**, 593-616.

ROBERTS, R.G. (1987): Ore deposit models. 11. Archean lode gold deposits. *Geosci. Can.* **14**, 37-52.

ROEDDER, E. (1984): Fluid Inclusions (P.H. Ribbe, ed.). *Rev. Mineral.* **12**.

ROMBERGER, S.B. (1986): The solution chemistry of gold applied to the origin of hydrothermal deposits. *In* Gold in the Western Shield (L.A. Clark, ed.). *Can. Inst. Min. Metall., Spec. Vol.* **38**, 168-186.

SABOIA, L.A. (1979): Os "Greenstone Belts" de Crixás e Goias - Go. *Sociedade Brasileira de Geologia, Boletim Informativo* **9**, 45-72.

______, TEIXEIRA, N.A, DE CASTRO, J.H. & TEIXEIRA, A.S. (1981): Geologia do "Greenstone Belt" de Crixás (Go) e suas implicacoes geotectonicas. *In* Anais 1 do Simposio sobre o Craton do Sao Francisco e suas Faixas Marginais. *Sociedade Brasileira do Geologia*, 39-50.

SCHOBBENHAUS, C., CAMPOS, D. DE A., DERZE, G.R. & ASMUS, H.E., co-ordinators (1984): Geologia do Brasil; Texto Explicativo do Mapa Geologico do Brasil e da Area Oceanica Adjacente includindo Depositos Minerais. (Escala 1:2,500,000). Departamento Nacional da Producao Mineral, Brasilia, Brasil.

TASSINARI, C.C.G. & MONTALVAO, R.M.G. (1980): Estudo geochronologico do "greenstone belt" Crixás. *Anais XXXI Congresso Brasileiro Geologia, Camboriu*, 2752-2759.

TEIXEIRA, N.A., SABOIA, L.A., FERREIRA, M.C.B., TEIXEIRA, A.S. & CASTRO, J.J.G. (1981): Estruturas e texturas das lavas ultrabasicas e basicas do greenstone belt de Crixás-Goias, Brasil. *Sociedade Brasileira de Geologia Nucleo Centro-Oeste* **10**, 38-87.

THOMSON, M.L. (1986): Petrology of the Crixás Gold Deposit, Brazil: evidence of gold associated with hydrothermal alteration subsequent to metamorphism. *In* Proc. Gold'86, an International Symp. on the Geology of Gold (A.J. Macdonald, ed.). Toronto, Ontario (284-296).

______ (1987a): *The Crixás Gold Deposit, Brazil: Metamorphism, Metasomatism and Gold Mineralization.* Ph.D. thesis, Univ. Western Ontario, London, Ontario.

______ (1987b): Progressive carbonatization of an epidote-amphibolite assemblage within the Crixás gold deposit, central Brazil. *Geol. Soc. Am., Abstr. Programs* **19**, 868.

______ (1991): Multiphase deformation and metamorphism of the Crixás greenstone belt, Goias, Brazil - evidence from poikiloblast inclusion trails. *J. South Am. Earth Sci.* (in press).

______ & FYFE, W.S. (1990): The Crixás gold deposit, Brazil: thrust related, post peak metamorphic gold mineralization of possible Brasilino Cycle age. *Econ. Geol.* **85**, 928-942.

WILLIAMS, P.J. (1990): Evidence for a late metamorphic origin of disseminated gold mineralization in

Grenville gneisses at Calumet, Quebec. *Econ. Geol.* **85**, 164-171.

WINKLER, H.G.F. (1974): *Petrogenesis of Metamorphic Rocks.* Springer-Verlag, New York.

Received May 20, 1990, revised manuscript accepted March 14, 1991.